Organic Geochemistry 40 (2009) 416–427

Contents lists available at ScienceDirect

Organic Geochemistry

journal homepage: www.elsevier.com/locate/orggeochem

Thermal decomposition process in algaenan of *Botryococcus braunii* race L. Part 2: Molecular dynamics simulations using the ReaxFF reactive force field

Elodie Salmon [a], Adri C.T. van Duin [b], François Lorant [a], Paul-Marie Marquaire [c], William A. Goddard III [b,*]

[a] Institut Français du Pétrole, BP 311, 92506 Rueil-Malmaison cedex, France
[b] California Institute of Technology, Materials and Process Simulation Center (MC139-74), 1200 East California Blvd., Pasadena, CA 91125, USA
[c] Département de Chimie Physique des Réactions, Nancy Université, CNRS, 1 rue Grandville, B.P.20451 F, 54001 Nancy cedex, France

ARTICLE INFO

Article history:
Received 15 May 2008
Received in revised form 16 August 2008
Accepted 27 August 2008
Available online 17 October 2008

ABSTRACT

This paper reports ReaxFF MD simulation results on pyrolysis of a molecular model of the algaenan *Botryococcus braunii* race L biopolymer, specifically, ReaxFF predictions on the pyrolysis of prototypical chemical structures involving aliphatic chain esters and aldehydes. These preliminary computational experiments are then used to analyze the thermal cracking process within algaenan race L biopolymers. The simulations indicate that the thermal decomposition of the algaenan biopolymer is initiated by the cleavage of a C–O bond in the ester group, followed by the release of carbon dioxide. We also observe a significant, strongly temperature dependent, release of ethylene. This degradation mechanism leads to products similar to those observed in pyrolysis experiments, validating this computational approach.

1. Introduction

It is now widely agreed that the combined effects of temperature and time on fossil organic matter initiate the processes that generate oil and gas in the subsurface, and that this thermal process can be described in terms of kinetic concepts. Understanding these chemical processes is necessary for properly modeling and predicting hydrocarbon generation in basin simulators. Our goal is to obtain a fundamental physico-chemical description of organic matter decomposition to provide a basis for estimating the quantity and quality of hydrocarbon formation in source rocks. The relevant rates and mechanisms are difficult to determine experimentally because the pyrolytic reactions that take place at low temperature over very large periods are not necessarily replicated in the laboratory.

Initially, kinetic models were used in experiments to estimate hydrocarbon potential (e.g. Huck and Karweil, 1955; Karweil, 1955; Vassoevich et al., 1969; Lopatin, 1971; Waples, 1980). Later, Tissot (1969, 1973) proposed a computational mathematical model using physico-chemical concepts to predict petroleum generation for petroleum exploration.

In the 1980s, new geochemical models were developed with the intent to quantify not only petroleum potential but also to estimate oil and gas quality. Solomon et al. (1988) proposed a mechanistic model to determine generation of oil, gas, char and tar fractions from coals. This model was based on a structural model of kerogen constrained by experimental analysis. In this model, the thermal decomposition is controlled by radical reactions kinetically derived from thermal decomposition of model compounds. Savage and Klein (1989) used a similar approach to describe the maturation of asphalthene. Their initial structural model of asphalthene was defined by stochastic methods. These studies demonstrated that this mechanistic approach provides both an estimate of oil and gas generation and a description of the residual structure of the kerogen in geological or laboratory context. However, the complex and heterogeneous structure of the kerogen cannot be represented by such model compound structures. Payne and Ortoleva (2002a) demonstrated that the diversity of representative structures of kerogen is more important than the size of the initial structural model.

More recently, Kelemen and co-workers (Kelemen et al., 2004; Freund et al., 2007) used a stochastic computational method to manage the chemical properties of the kerogen and defined a two dimensional complex macro-model. Kinetically constrained radical reactions were employed to reproduce the thermal decomposition of the type II kerogen structure. This approach proposed that both kinetic properties and the structural model are derived partially or entirely from a set of elemental reactions initially defined by experimental and geological observations. Thus, production of hydrocarbons is obtained by a stochastic distribution of the radical reactions for a given thermal history, while constrained by the physico-chemical properties of the structural model.

Recent decades have seen increasing use of theory to elucidate mechanisms and rates of chemical processes. Reliable theory requires very large scale quantum mechanics (QM) on systems far too small (~100 atoms) to accurately represent the

* Corresponding author. Tel.: +1 626 395 2731; fax: +1 626 585 0918.
E-mail addresses: wag@wag.caltech.edu, shirley@wag.caltech.edu (W.A. Goddard).

0146-6380/$ - see front matter © 2008 Elsevier Ltd. All rights reserved.
doi:10.1016/j.orggeochem.2008.08.012

transformations of sedimentary organic matter, which might require 1000s to millions of atoms. A recent breakthrough in the methods for predicting reaction mechanisms and rates from first principles (the ReaxFF reactive force field) allows reacting systems to be described with accuracy close to QM, but with the computational costs reduced many orders of magnitude. With the development of the ReaxFF reactive force field by van Duin et al. (2001), it is now practical to consider MD (molecular dynamics) simulations as an alternative technique for describing the stability and geometry of small and medium size hydrocarbon systems (C_{1000} to $C_{1,000,000}$) for a modest period of time (100 ns), coupling MD with chemical reactions. ReaxFF MD allows accurate simulations of chemical reactions for size and timescales sufficient to describe reactivity and identify reaction pathways of complex chemical systems (e.g. Van Duin and Sinninghe Damsté, 2003; Strachan et al., 2003; Chenoweth et al., 2005, 2008; Chen et al., 2005; van Duin et al., 2005; Han et al., 2005; Buehler et al., 2006; Goddard et al., 2006a,b; Ludwig et al., 2006) and to define kinetic parameters (Chenoweth et al., 2005; Leininger, 2007; Leininger et al.,2008).

Here we apply ReaxFF MD to provide a detailed analysis of simulation results that allows us to derive the key mechanistic steps responsible for the reactivity trends, providing the basis for a bulk kinetic model useful for basin modeling. This computational approach allows thermal cracking of organic matter to be studied without any assumption on the nature of reaction mechanisms. All that is needed is a structural model representative of the kerogen to perform the simulations. In this study, we selected a well defined end member biopolymer, algaenan, to represent the kerogen structure. Based on both experimental analysis of samples and a model from the literature, an atomistic model for this biopolymer was defined in Salmon et al. (2009). We now use this model in ReaxFF simulations of thermal decomposition of algaenan race L material.

In a first series of simulations, we used a number of representative moieties (50 to 100 atoms) of the algaenan macro-model to set up the computational procedure and study the thermal decomposition process of specific algaenan substructures. Specific substructures (aliphatic and isoprenoic chain) and chemical functions (esters and aldehydes) were isolated from the algaenan macro-model and ReaxFF MD simulations were performed on those models for a range of volume and temperature conditions, providing details of the thermal decomposition process for each specific structure.

Thereafter, we describe how ReaxFF MD simulations are performed on a macro-model containing all the functionality of the algaenan polymer. Detailed reaction pathways of the decomposition of the functional model are used to describe the decomposition of the macro-model. These simulation results are then validated by comparison with theoretical thermal decomposition profiles and with experimental pyrolysis results obtained on algaenan race L sample (Salmon et al., 2009).

2. Methods

2.1. Selection of molecular models for algaenan

The algaenan race L, which is representative of aliphatic fossil organic matter, was selected for the present study. In a previous paper (Salmon et al., 2009), we proposed three dimensional molecular models of the initial algaenan samples. These structures were derived from models found in the literature (Berthéas et al., 1999) and constrained by experimental characterization (elemental analysis, IR spectra, ^{13}C NMR). The macro-model of algaenan, composed of 2966 atoms, is a linear extension of the structural model proposed by Salmon et al. (2009). The biopolymer contains eight C_{31} aliphatic chains substituted by an aldehyde group and ten C_{31} aliphatic chains substituted by an ester functional group and a C_{40} isoprenoid chain (Fig. 1). This macro-model was built using Cerius^2 (version 4.8.1, Accelrys software) and minimized with UFF_VALBOND 1.1 (a combination of the original VALBOND method described by Root et al. (1993), augmented with non-orthogonal strength functions taken from Root (1997) and the Universal Force Field of Rappé et al. (1992)). Functional models composed of 50 to 100 atoms were selected to represent specific chemical groups of the algaenan macro-model (Fig. 1). The first one, composed of 97 atoms ($C_{33}H_{62}O_2$), contains an ester functional group linked to both a C_{17} unsaturated aliphatic chain and a C_{15} isoterpenoid chain (Fig. 1C; we will refer to this as the ester model). The second one, composed of 53 atoms, represents a mono-unsaturated aliphatic chain conjugated to an aldehyde group ($C_{18}H_{34}O$, Fig. 1D, we will refer to this as the aldehyde model).

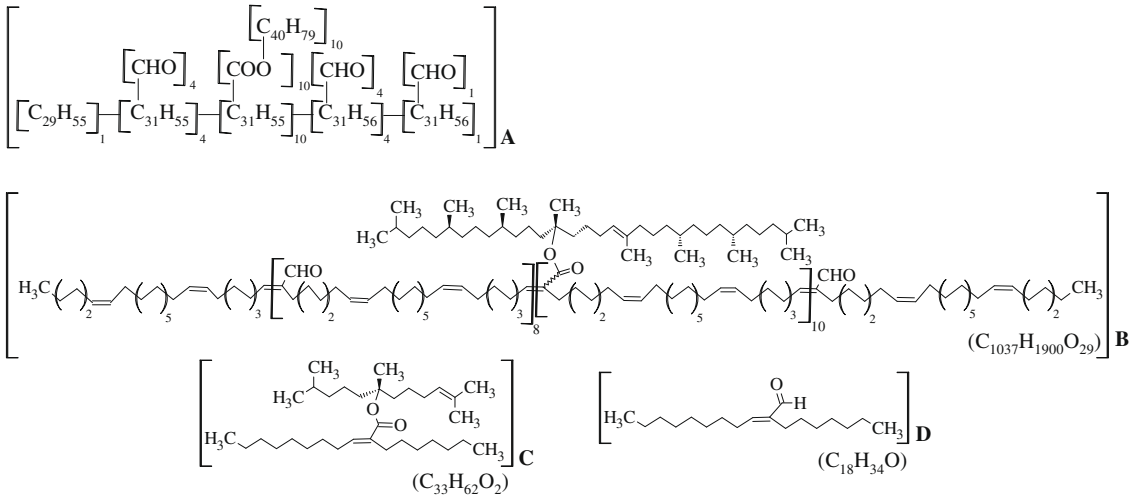

Fig. 1. (A) Simplified representation of the aldehyde and ester groups in the algaenan macro-structural. (B–D) Full atomistic representation of the algaenan macro-model (B) and the ester (C) and aldehyde (D) functional models.

2.2. The ReaxFF reactive force field

The ReaxFF (van Duin et al., 2001) reactive force field is a first principles force field whose parameters are derived solely from a large database of quantum mechanical (QM) calculations on a large number of organic reactions, including both ground states and transition states. ReaxFF is many orders of magnitude simpler and cheaper than QM which has allowed practical molecular dynamics (MD) simulations on the decomposition, reactions, and oxidations of systems with 100,000–1,000,000 atoms over a range of temperatures, pressures and compositions. The equations of motion in ReaxFF are derived from a Hamiltonian in which the potential energy is partitioned into contributions from valence, electrostatic and van der Waals interaction, as with ordinary FF, but we allow the bond orders and charges to change as the geometric structure evolves from reactants to intermediates to products. The bond order/bond distance relationship allows smooth transition from non-bonded to bonded systems (Tersoff, 1988; Brenner, 1990). At every iteration of the MD, the bond orders and charges are updated. All valence interactions (including angle bending, torsion and inversion) depend on bond order, so that their energy contributions disappear upon bond dissociation. The electrostatic (Coulombic) interactions between atoms are properly shielded to remain finite for short distances. These charge transfer effects are described using the EEM method (Mortier et al., 1986) of describing the dependence of charge on geometry, similar to but simpler than the Charge Equilibration (QEq) method (Rappé and Goddard, 1991). This study uses the H/C/O ReaxFF parameters as reported recently by Chenoweth et al. (2008).

2.3. Simulation procedure

The simulations on the ester and aldehyde models described in Section 2.1 were managed according to the following scheme (see Fig. 2):

(1) To initiate the simulations we build a periodic cubic box containing either 5 copies of the ester or 10 copies of the aldehyde model at a low density (<0.1 kg dm^{-3}). Each box contains around 500 atoms (Table 1).

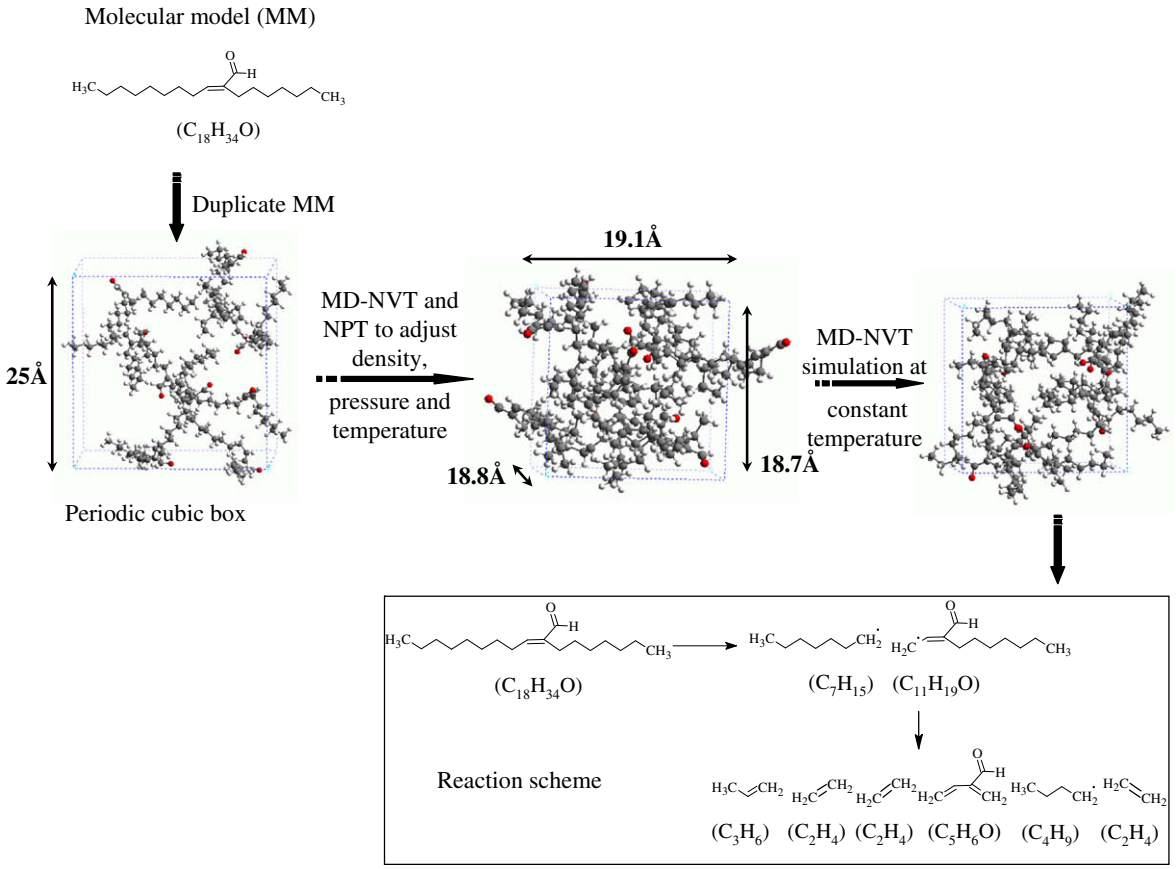

Fig. 2. Simulation procedure used to define physico-chemical properties and observed thermal decomposition of the structural models. MM, molecular model; MD, molecular dynamics; NVT, simulation with fixed number of atoms, volume and temperature; NPT, simulation with fixed number of atoms, pressure and temperature.

Table 1
Simulation conditions for the constant temperature NVT-MD simulations obtained at the end of the simulation procedure (Fig. 2).

Models			Initial model		Density (kg dm^{-3})	Volume (Å^3)
			Nr of atoms per model	Nr of models per simulation		
Macro-model	B	Algaenan	2966	1	0.57	43026
Functional	C	Ester	97	5	0.69	5890
models	D	Aldehyde	53	10	0.66	6732

(2) Subsequently, a low temperature (2 K) molecular dynamics was performed on this initial low density configuration. Thereafter, the system was equilibrated at a fixed volume using the Berendsen thermostat (Berendsen et al., 1984) to maintain the temperature at 300 K. Such simulations are denoted as NVT-MD. These NVT simulations were initially carried out for 2.5 picoseconds. This system was then compressed to the experimental solid density at room temperature of $d = 1.2\ \mathrm{kg\,dm^{-3}}$ by means of re-scaling the cell parameters during a 1.25 ps MD simulation at $T = 300$ K. Thereafter the system was equilibrated at a pressure of 1 bar and a temperature of 750 K. Here, the volume was allowed to change in such a way that the pressure was maintained at 1 atm using the Berendsen barostat. Such MD simulations to maintain a specified pressure and temperature (but fixed numbers of atoms) are denoted as NPT MD. These NPT simulations were carried for 25 ps during which time the system expands to about $0.7\ \mathrm{kg\,dm^{-3}}$.

(3) Thereafter, heat up simulations were performed for the functional model from 300 to 2500 K at rates of 88, 44, and 22 K/ps (Fig. 3) to determine the onset temperature of thermal decomposition at the picosecond time scale of our simulations.

The thermal decomposition of functional models began between 1700 and 2500 K and the macro-model at around 1500 K. To determine the kinetics of the thermal decomposition reactions, we performed constant temperature molecular dynamics simulations for both functional models for 50 ps at $T = 2000$, 2100 and 2200 K.

The time scale of the simulation, (50 ps), is much shorter than that of the experiments (9 hours; Salmon et al., 2009). Thus, in the simulations we increase the temperature from the 473 to 573 K range used in experiments to 2000–2200 K to allow chemical reactions to be observed on the computational time scale. This difference in time and temperature scales between simulation and experiment may certainly affect product distributions, but we ex-

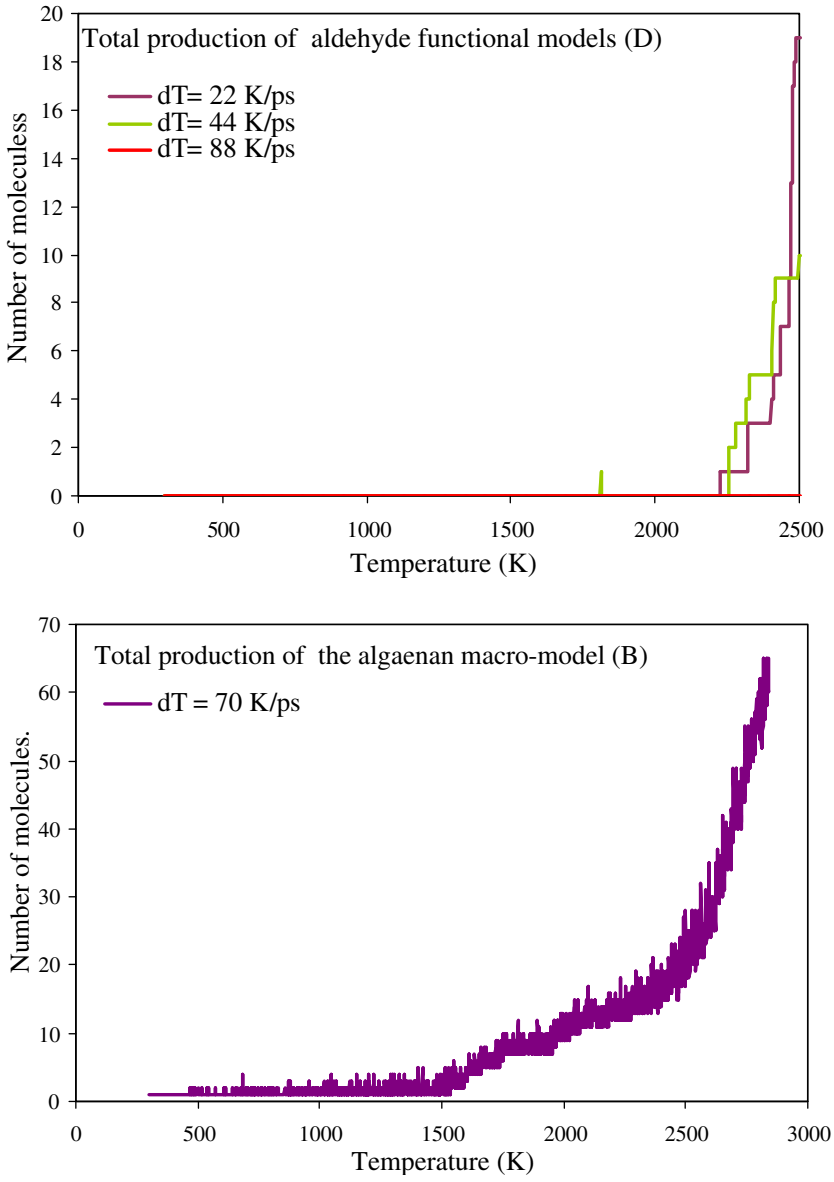

Fig. 3. Total molecular fragment production for the aldehyde functional model (on the top) and the algaenan macro-model (on the bottom) as observed during simulations using heat up rates of 22, 44, and 88 K/ps (aldehyde) and 70 K/ps (algaenan).

pect to find qualitative agreement in the initial decomposition processes. It might be possible to reduce the temperature gap between simulation and experiment by using improved transition state sampling (e.g. Chopra et al., 2008) or by using external forces to drive the reactions and measure transition state energies; however such methods should be carefully formulated to avoid systematic bias.

For the macro-model, we employed a similar strategy (build at low density, compress to experimental density, and heat up to find initiation temperature). The heat up simulation was performed from 300 K to 2800 K at a rate of 70 K/ps (Fig. 3). Thereafter, NVT-MD was carried for 40 ps at $T = 1500$, 1600, 1700, 1800, 1900 and 2000 K.

3. Results

3.1. Thermal decomposition of ester and aldehyde functional models of algaenan

Fig. 4 shows the thermal decomposition of the ester and aldehyde functional models. We observe that the ester models are rapidly degraded in less than 10 ps at all temperatures. The aldehyde model is more resistant and takes 50 ps at 2200 K to degrade fully. Structural analysis of the simulated thermal degradation shows that the decomposition of the ester model starts by the release of the $C_{15}H_{29}$ side chain, followed by β-scission reactions resulting in the depolymerization of the aliphatic chains. At the same time, defunctionalization of the ester radical results in the generation of CO_2, as displayed in Fig. 5C. We observe that the thermal decomposition of the aldehyde functional model does not generate carbon monoxide. Only depolymerization of the aliphatic chain is obtained by successive β-scission reactions (Fig. 5D). In both models, unsaturated species are generated mainly by β-scission reactions; the high temperature simulations also show a few dehydrogenation events. Table 2 shows the final chemical composition of the simulations for both models. We observe that with increasing temperature more lightweight ($<C_6$) products are generated. At $T = 2000$ and 2100 K recombination reactions between C_{18} and C_6 alkyl products generate longer alkyl chains containing 24 carbons. Apart from carbon dioxide, we also obtain minor amounts of H_2O and H_2 by β-scission and metathesis reactions.

3.2. Reproducibility of functional model results

The molecular dynamics scheme employed here is based on deterministic Newtonian motion enabling us to describe the femtosecond dynamics of a molecular scale system. Consequently, the final results obtained at the end of a given simulation time depend only on the initial pressure, temperature and initial atom positions and velocities. Since we are sampling rare, reactive events, multiple simulations, starting from equivalent initial configurations, are required to check the statistical reliability of the simulation results. For each functional model, as defined in Fig. 1, we constructed periodic boxes containing 5 to 10 duplicates, depending on the model size (Table 1).

To test the reproducibility of the results described in the previous section, we repeated the functional model simulations with five independent start configurations. Fig. 6 displays the reproducibility results for the decomposition and total production of the ester functional model for five initial configurations at three temperatures ($T = 2000$, 2100 and 2200 K). We observed a slight variation of the decomposition. Total decomposition of the five functional models occurred after 4 to 11 ps, 3 to 14 ps, and 3 to 6 ps of simulation at 2000, 2100 and 2200 K, respectively. The total production has a higher variation than the decomposition, after 50 ps, 21 to 27 molecules, 19 to 32 molecules, and 11 to 21 molecules were generated at $T = 2000$, 2100 and 2200 K, respectively. Analysis of the chemical composition during the simulations allows us to identify the reproducibility of the reactions mechanism. Table 3 reports the maximum and minimum occurrence of each molecule as observed during the five independent simulations at $T = 2000$, 2100 and 2200 K after 14 ps and 50 ps. The chemical composition observed after 14 ps of decomposition shows only primary reaction products, while the composition after 50 ps is dominated by secondary reactions. As an example of this, at 2000 K/14 ps and 2100 K/14 ps, the ester functional model $C_{33}H_{62}O_2$ was merely decomposed to $C_{18}H_{33}O_2$ and $C_{15}H_{29}$. At higher temperature (2200 K/14 ps) more rapid secondary reactions occur, producing $C_{11}H_{20}$ and CO_2. After 50 ps at all temperatures, the primary reaction products $C_{18}H_{33}O_2$ and $C_{15}H_{29}$ are transformed into molecules of smaller sizes. Main molecules produced were $C_{17}H_{33}$, $C_{11}H_{20}$, $C_{10}H_{18}$, C_9H_{18}, C_3H_7, C_2H_4, and CO_2. To summarize, while we observe a significant spread in the decomposition time and production rate during the five independent simulations, the chemical mechanisms are well reproduced. Furthermore, while there is no statistically clear relationship observed between decomposition/production rate and temperature, we do observe a clear and reproducible impact of the temperature on the nature of the chemical events. Due to the rarity of the chemical events, more independent (or larger) simulations are required to fully sample these rare events and consequently quantify reaction rates.

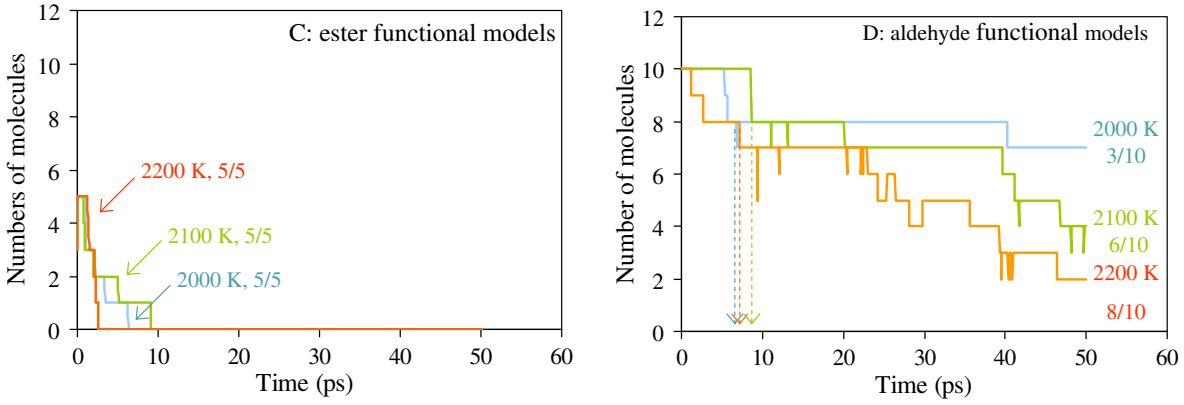

Fig. 4. Thermal decomposition yield for the ester (C) and aldehyde (D) functional models.

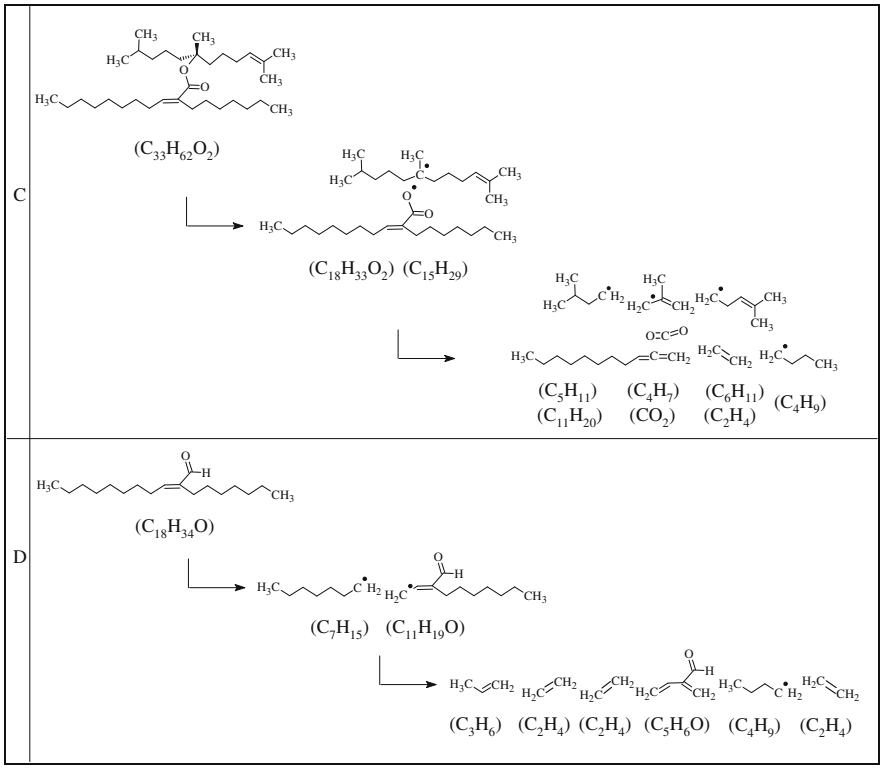

Fig. 5. Main decomposition reactions observed during the NVT-MD simulation of the ester functional models (C) and of the aldehyde functional models (D).

Table 2
Chemical composition observed after 50 ps of NVT-MD simulation at 2000, 2100, and 2200 K for the ester and the aldehyde functional models.

	Ester functional model (C) $5\times C_{33}H_{62}O_2$			Aldehyde functional model (D) $10\times C_{18}H_{34}O$		
	2000 K/50 ps	2100 K/50 ps	2200 K/50 ps	2000 K/50 ps	2100 K/50 ps	2200 K/50 ps
C_{6+}hydrocarbons	$C_{24}H_{46}O_2$	$C_{24}H_{44}O_2$		6 $C_{18}H_{34}O$	4 $C_{18}H_{34}O$	$C_{18}H_{34}O$
	$C_{18}H_{33}O_2$	2 $C_{18}H_{33}O_2$	$C_{18}H_{33}O$	2 $C_{12}H_{21}O$	$C_{12}H_{21}O$	$C_{12}H_{21}O$
	$C_{17}H_{33}$	Ci_4H_{26}	$C_{15}H_{28}$	$C_{11}H_{19}O$	$C_{15}H_{27}O$	$C_{18}H_{33}O$
	$C_{11}H_{20}$	$2C_{11}H_{20}$	3 $C_{11}H_{20}$		$C_{11}H_{20}O$	$C_{17}H_{31}O$
	$C_{12}H_{20}O_2$	$2C_9H_{18}$	$C_{10}H_{18}$		$C_{11}H_{20}$	$C_{13}H_{23}O$
	$C_{10}H_{20}$	C_9H_{17}	2 $C_{10}H_{17}$			$C_{11}H_{20}O$
	2 $Ci_{10}H_{18}$		C_8H_{12}			C_7H_{16}
	C_9H_{18}					
	C_9H_{17}					
C_{6-}hydrocarbons	C_6H_{10}	C_6H_{12}	C_6H_{12}		C_6H_8O	C_6H_{12}
	C_6H_{11}		C_6H_{13}	C_6H_{13}		
			C_6H_{14}		C_5H_6O	3 C_5H_6O
	C_5H_9		C_5H_{10}		C_5H_{10}	
	CsH_{12}		C_4H_{10}		C_5H_{12}	
	C_4H_8	2 C_4H_8	C_4H_8		C_4H_8O	
		C_4H_7	C_4H_7		C_4H_6	
		C_4H_6	C_4H_6		C_3H_6	$3C_3H_6$
		C_3H_7	C_3H_7	C_3H_7		C_3H_7
		C_2H_5	C_2H_5	C_2H_5	3 C_2H_5	2 C_2H_5
	3 C_2H_4	6 C_2H_4	5 C_2H_4	5 C_2H_4	10 C_2H_4	16 C_2H_4
				C_2H_3		
	CH_3				CH_3	2 CH_3
		CH_4	CH_4			CH_4
Others	2 CO_2	2 CO_2	4 CO_2			
			H_2O			
	H_2		$2H_2$		H_2	H_2

3.3. Thermal decomposition of the macro-model of algaenan

A heat up simulation of the algaenan race L macro-model was performed to obtain an overview of the decomposition process. Fig. 7 shows the time evolution of the products obtained from the thermal decomposition of the biopolymer. Using a heating rate of 70 K/ps, we find that degradation of the macro-structure initiates at about 1400 K. As in the functional model simulations,

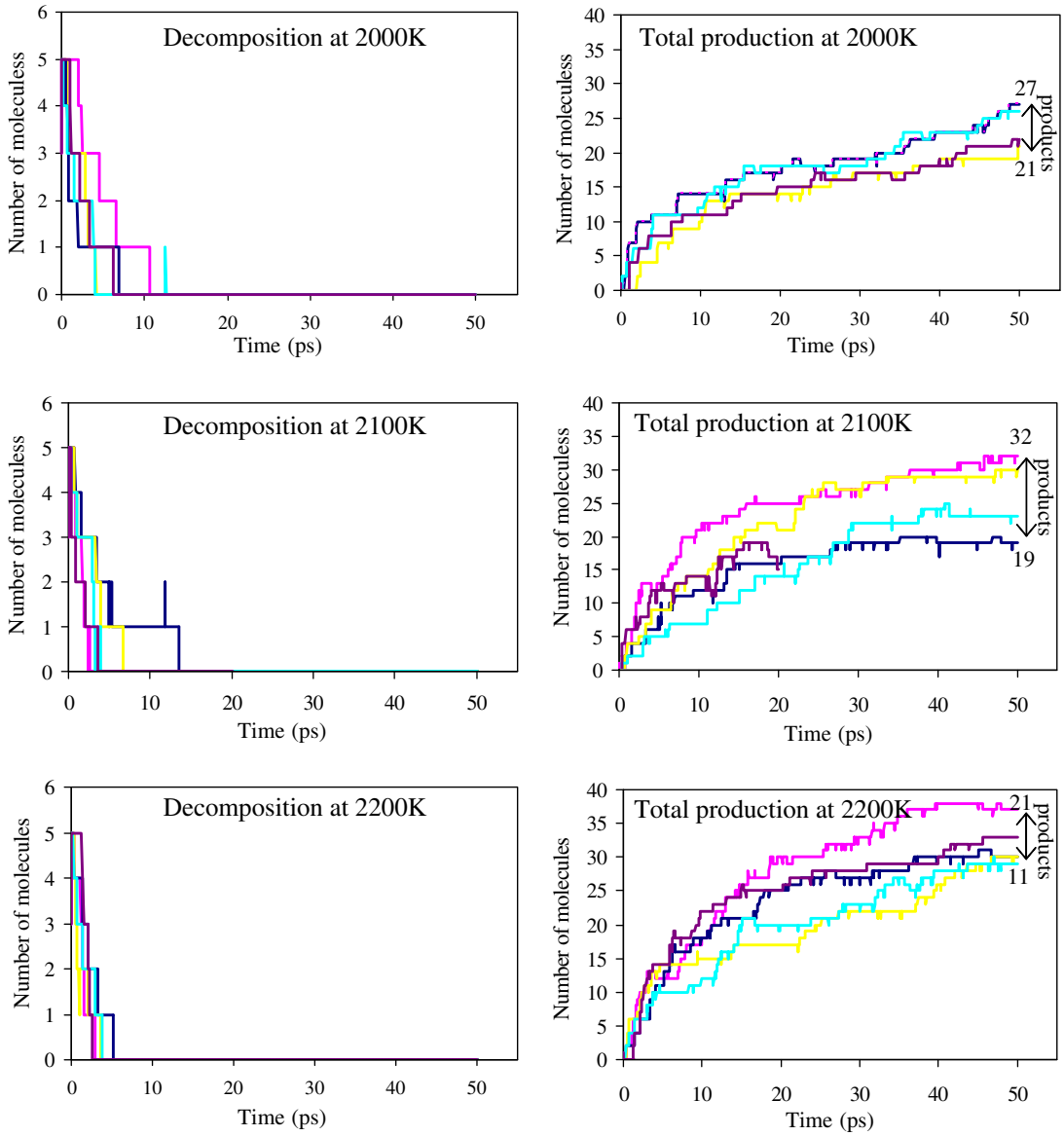

Fig. 6. On the left: decomposition and total production obtained by NVT-MD simulations at 2000, 2100 and 2200 K, of five independent configurations of the ester functional models. On the right: Global composition obtained after 50 ps of simulated thermal decomposition for five independent initial configurations.

the side chain ($C_{40}H_{79}$) is first released as a result of the thermal stress. Thereafter, carbon dioxide and ethene appear at around 1900–2000 K and 2300 K, respectively. To analyze the details of the decomposition process, a series of 6 NVT-MD simulations were performed for 40 ps for temperatures of 1500, 1600, 1700, 1800, 1900 and 2000 K. A pressure evolution of the system has been performed for the simulation at 2000 K. The pressure, initially at 0.21 Gpa (±0.04), increases to reach 0.31 GPa (±0.05) at the end (t = 37 ps) of the simulation. Fig. 8 shows a detailed analysis of the production of the side chain ($C_{40}H_{79}$), carbon dioxide and ethene. We observe that initiation reactions generate up to nine $C_{40}H_{79}$ radicals; secondary reactions degrade these radicals at longer times and higher temperatures. During the NVT-MD simulation at 1500 K, only one carbon dioxide is generated. Increasing thermal stress causes CO_2 to appear earlier and to become more frequent; at T = 2000 K production began at 4 ps and a total of seven CO_2 molecules were generated at t = 32 ps. We observe the strongest temperature dependence in the ethene production. At T = 1800 K and T = 1900 K, respectively, three and four ethene molecules are produced, but at T = 2000 K, a sharp increase of ethene production is noted, resulting in the formation of 18 ethene molecules generated during the 40 ps of simulation. Analyses of trajectory provided by the simulations show that carbon dioxide originated from the cleavage of the ester function after the release of the C_{40} side chain (Fig. 9). Four β-scission reactions, as depicted in Fig. 10, are at the origin of the decomposition of the C_{40} radical. A complete list of the products observed in those simulations is provided in Table 4. Isoprenoid moieties, noted by a star, are dominant in the C_6–C_{40} compounds. Ethene and carbon dioxide are the main products in the low molecular weight fraction.

4. Discussion and conclusion

The ReaxFF MD simulations provide detailed reaction schemes for the thermal decomposition of both specific functional models and for a macro-structure of algaenan race L. In both the functional

Table 3
Minimum and maximum occurrence (min-max) of initial compounds and decomposition products observed at 2000, 2100, and 2200 K by thermal decomposition of five independent initial configurations of the ester functional model. Chemical compositions are listed after 14 and 50 ps of NVT-MD simulations; key compounds are depicted in bold.

Ester functional models (C) 5 × $C_{33}H_{62}O_2$											
2000 K/14 ps		2100 K/14 ps		2200 K/14 ps		2000 K / 50 ps		2100 K/50 ps		2200 K/50 ps	
(0–1)	$C_{18}H_{34}O_2$	(0–2)	$C_{18}H_{34}O_2$	(0–1)	$C_{19}H_{35}O_2$	(0–1)	$C_{24}H_{46}O_2$	(0–1)	$C_{26}H_{46}O_2$	(0–1)	$C_{18}H_{34}O_2$
(3–5)	**$C_{18}H_{33}O_2$**	**(2–5)**	**$C_{18}H_{33}O_2$**	(0–1)	$C_{18}H_{34}O_2$	(0–1)	$C_{19}H_{37}O_2$	(0–1)	$C_{24}H_{44}O_2$	(0–1)	$C_{18}H_{33}O_2$
(0–1)	$C_{18}H_{33}O$	(0–1)	$C_{11}H_{19}O_2$	**(1–2)**	**$C_{18}H_{33}O_2$**	(0–2)	$C_{18}H_{34}O_2$	(0–1)	$C_{20}H_{38}O_2$	(0–1)	$C_{18}H_{33}O$
(0–1)	$C_{17}H_{33}O$	(0–1)	$C_{11}H_{18}O_2$	(0–1)	$C_{18}H_{31}O_2$	(0–1)	$C_{18}H_{33}O_2$	(0–2)	$C_{18}H_{34}O_2$	(0–1)	$C_{12}H_{20}O_2$
(0–1)	$C_{15}H_{30}O$	(0–1)	$C_{17}H_{33}$	(0–1)	$C_{16}H_{28}O_2$	(0–1)	$C_{18}H_{33}O$	(0–2)	$C_{18}H_{33}O_2$	(0–1)	$C_{11}H_{18}O$
(0–1)	$C_{17}H_{33}$	**(1–2)**	**$C_{15}H_{29}$**	(0–1)	$C_{14}H_{24}O_2$	(0–1)	$C_{17}H_{34}O$	(0–1)	$C_{14}H_{25}O_2$	(0–1)	$C_{17}H_{33}$
(1–3)	**$C_{15}H_{29}$**	(0–1)	$C_{15}H_{28}$	(0–1)	$C_{12}H_{21}O_2$	(0–1)	$C_{15}H_{30}O$	(0–1)	$C_{11}H_{19}O_2$	(0–1)	$C_{15}H_{28}$
(0–1)	$C_{10}H_{20}$	(0–1)	$C_{14}H_{26}$	(0–1)	$C_{17}H_{33}$	(0–1)	$C_{13}H_{22}O_2$	(0–1)	$C_{28}H_{28}$	(0–1)	$C_{14}H_{27}$
(0–2)	$C_{10}H_{18}$	(0–2)	$C_{11}H_{20}$	(0–2)	$C_{15}H_{29}$	(0–1)	$C_{12}H_{20}O_2$	(0–1)	$C_{14}H_{26}$	(0–1)	$C_{14}H_{26}$
(0–1)	C_9H_{18}	(0–1)	$C_{10}H_{20}$	(0–2)	C_5H_{28}	(0–2)	$C_{11}H_{18}O_2$	(0–3)	$C_{11}H_{20}$	(0–1)	$C_{13}H_{24}$
(0–1)	C_9H_{16}	(0–3)	$C_{10}H_{18}$	(0–1)	$C_{14}H_{26}$	**1**	**$C_{17}H_{33}$**	(0–1)	$C_{11}H_{19}$	(0–1)	$C_{12}H_{22}$
(0–1)	C_6H_{11}	(0–1)	$C_{10}H_{17}$	**(1–2)**	**$C_{11}H_{20}$**	(0–1)	$C_{15}H_{28}$	(0–1)	$C_{10}H_20$	(0–2)	$C_{11}H_{21}$
(0–1)	C_6H_{10}	(0–2)	C_9H_{18}	(0–2)	$C_{10}H_{18}$	(0–1)	$C_{15}H_{25}$	(0–3)	$C_{10}H_{18}$	(2–4)	$C_{11}H_{20}$
(0–2)	C_5H_{11}	(0–1)	C_9H_{17}	(0–1)	$C_{10}H_{17}$	**(1–2)**	**$C_{11}H_{20}$**	**(1–4)**	**C_9H_{18}**	(0–1)	$C_{10}H_{20}$
(0–1)	C_5H_9	(0–1)	C_7H_{15}	(0–3)	C_9H_{18}	(0–1)	$C_{10}H_{20}$	(0–1)	C_9H_{17}	(0–1)	$C_{10}H_{19}$
(0–1)	C_4H_9	(0–1)	C_7H_{14}	(0–1)	C_9H_{16}	(1–3)	$C_{10}Hi_8$	(0–1)	C_8H_{18}	(0–2)	$C_{10}H_{18}$
(0–1)	C_4H_7	(0–2)	C_6H_{13}	(0–1)	C_6H_{13}	(0–2)	C_9H_{18}	(0–1)	C_8H_{14}	(0–2)	$C_{10}H_{17}$
(0–1)	C_3H_7	(0–2)	C_6H_{11}	(0–1)	C_6H_{12}	(0–1)	C_9H_{17}	(0–1)	C_7H_{14}	(0–4)	C_9H_{18}
(0–1)	C_3H_6	(0–3)	C_5H_{11}	(0–1)	C_6H_{11}	(0–1)	C_9H_{16}	(0–1)	C_6H_{14}	(0–1)	C_8H_{16}
(0–2)	C_2H_4	(0–1)	C_5H_9	(0–3)	C_5H_{11}	(0–1)	C_8H_{17}	(0–1)	C_6H_{12}	(0–1)	C_8H_{12}
(0–1)	CO_2	(0–1)	C_4H_9	(0–1)	C_5H_{10}	(0–1)	C_8H_{16}	(0–1)	C_6H_{11}	(0–1)	C_7H_{15}
(0–1)	CO	(0–1)	C_4H_7	(0–1)	C_5H_9	(0–1)	C_7H_{14}	(0–2)	C_5H_{11}	(0–1)	C_6H_{14}
		(0–1)	C_3H_7	(0–1)	C_4H_9	(0–1)	C_6H_{13}	(0–1)	C_5H_9	(0–2)	C_6H_{13}
		(0–1)	C_3H_6	(0–1)	C_4H_8	(0–1)	C_6H_{12}	(0–1)	C_5H_8	(0–1)	C_6H_{12}
		(0–4)	C_2H_4	(0–1)	C_4H_7	(0–1)	C_6H_{11}	(0–1)	C_4H_{10}	(0–1)	C_6H_{11}
		(0–1)	CH_4	(0–1)	C_4H_6	(0–2)	C_6H_{10}	(0–2)	C_4H_8	(0–1)	C_5H_{12}
		(0–2)	CO_2	(0–2)	C_3H_7	(0–2)	C_5H_{11}	(0–1)	C_4H_7	(0–1)	C_5H_{11}
		(0–1)	H_2	(0–1)	C_3H_6	(0–1)	C_5H_9	(0–1)	C_4H_6	(0–1)	C_5H_{10}
				(0–1)	C_2H_5	(0–2)	C_5H_8	(0–1)	C_3H_8	(0–2)	C_5H_9
				(0–3)	C_2H_4	(0–1)	C_5H_{12}	**1**	**C_3H_7**	(0–1)	C_5H_8
				(0–1)	CH_3	(0–1)	C_4H_9	(0–2)	C_3H_6	(0–2)	C_4H_8
				(1–3)	**CO_2**	(0–1)	C_4H_8	(0–1)	C_3H_4	(0–1)	C_4H_7
				(0–3)	H_2	(0–1)	C_4H_7	(0–1)	C_2H_5	(0–1)	C_4H_6
						(0–1)	C_4H_5	**(3–8)**	**C_2H_4**	(0–1)	C_4H_{10}
						(0–2)	C_3H_7	(0–1)	CH_4	(0–1)	C_3H_7
						(0–2)	C_3H_6	(0–1)	CH_3	(0–4)	C_3H_6
						(0–1)	C_2H_5	(0–4)	CO_2	(0–1)	C_3H_4
						(2–5)	**C_2H_4**	(0–1)	H_2	(0–1)	C_3H_3
						(0–2)	CH_3			(0–1)	C_2H_5
						(2–4)	**CO_2**			**(5–12)**	**C_2H_4**
						(0–1)	CO			(0–1)	C_2H_3
						(0–6)	H_2			(0–1)	CH_4O
										(0–1)	CH_2O
										(0–1)	CH_4
										(0–4)	CH_3
										(3–5)	CO_2
										(0–1)	H_2O
										(0–2)	H_2

models and the macro-model, we observe that thermal decomposition of the algaenan structure initiates with the release of the isoprenoid side chain. Thereafter, the ester function cleaves to produce substantial amounts of carbon dioxide. At higher temperature we observe the generation of ethene as a result of successive β-cleavage reactions. In order to compare this reaction pathway with experimental observations, Table 5 reports time and temperature conditions for which main products are generated during heat up simulations, NVT-MD and experiments (Behar et al., 1995; Salmon et al., 2009). Despite the substantial difference between the numerical and experimental conditions, the order of generating the molecular species is the same. As a first approximation, we equate

- the C_{40+} compounds observed in the simulations to the experimental residue,
- the C_{14}–C_{40} compounds from the simulations to the experimental C_{14+} fraction,
- the C_6–C_{14} compounds from the simulations to the experimental C_6–C_{14} fraction, and
- the C_{6-} compounds from the simulation to the experimental gas fraction.

The main products observed at the end of the macro-model simulations are isoprenoid structures, carbon dioxide and at high temperature, ethene. This is in excellent qualitative agreement with the experimental results. Based on atomic ratios H/C and O/C, we compare chemical properties of the experimental residue with the C_{40+} compounds in the simulations. Fig. 11 displays the evolution of the atomic ratios with thermal stress, showing strong similarity between simulation and experiment. In both cases, the oxygen content of the initial structures is lower than that of the first residues. This agrees with the release of $C_{40}H_{79}$ isoprenoid side chains observed experimentally. Thus, a large amount of carbon and hydrogen is released while the oxygen content remains unchanged. Thereafter, the oxygen content

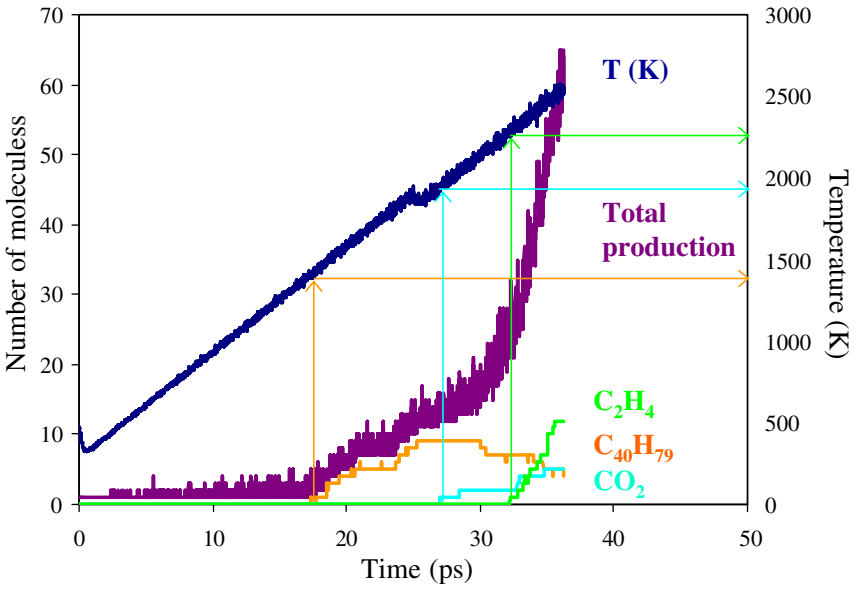

Fig. 7. Molecular fragments as a function of temperature for the algaenan macro-model at a heat up rate of 70 K/ps.

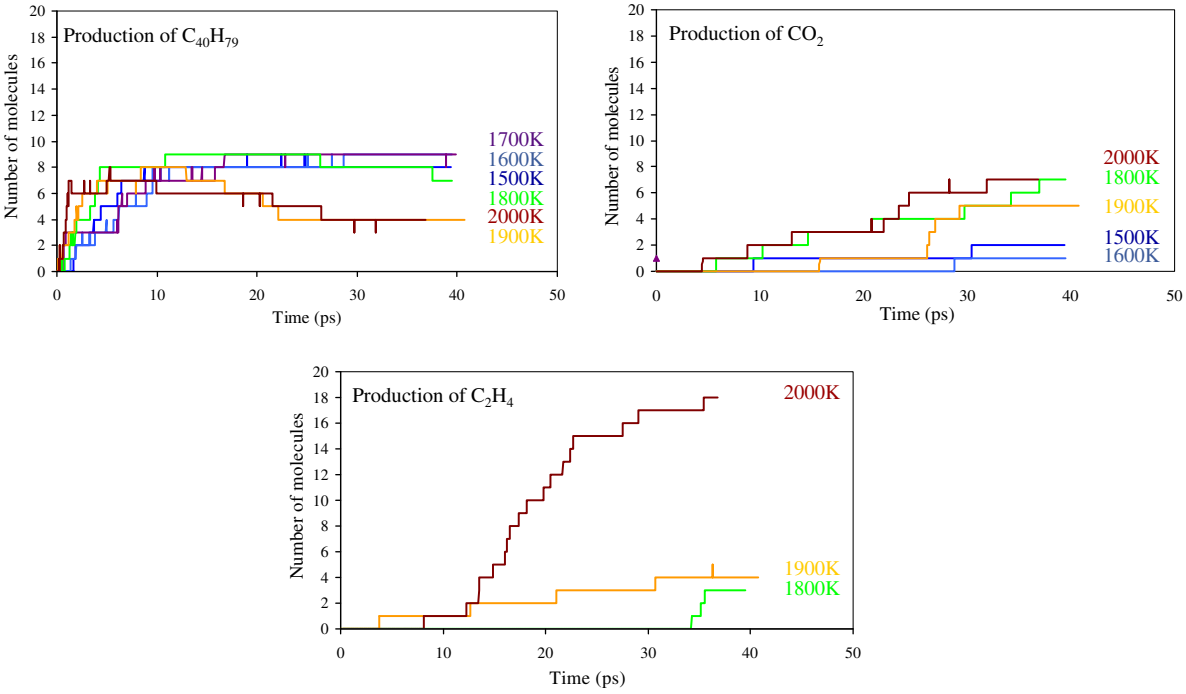

Fig. 8. Generation profile for $C_{40}H_{79}$, CO_2, and C_2H_4 observed at T = 1500, 1600, 1700, 1800, 1900 and 2000 K for the macro-model of algaenan.

decreases due to the formation of CO_2 from carboxyl groups. The large gap between the initial molecular model and the numerical C_{40+} compounds is due to the high temperature used for MD simulations, increasing the kinetics of the chemical process.

To conclude, MD modeling using the reactive force field ReaxFF successfully describes the initial chemical processes of thermal decomposition of the algaenan race L like aliphatic fossil organic matter. This study also shows that MD simulations performed on small structural functional models may be used to confirm chemical mechanisms of thermal decomposition. Finally, ReaxFF MD molecular modeling proves useful to infer and/or confirm the mechanisms underlying the chemical process of thermal decomposition. Thus, ReaxFF MD should be useful to understand the structural organization of the kerogen by retro-validation of the chemical processes.

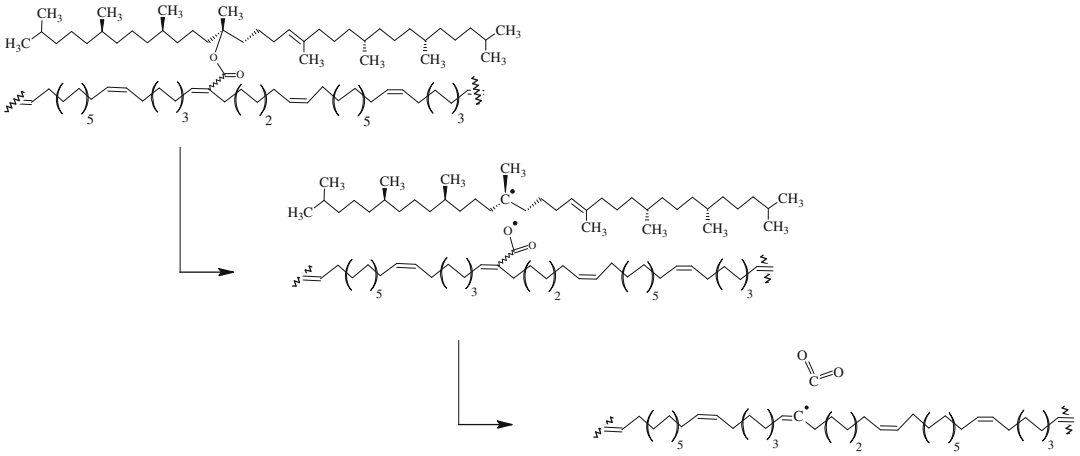

Fig. 9. Initial steps in the thermal decomposition of the algaenan macro-model as observed during the constant temperature NVT-MD simulations.

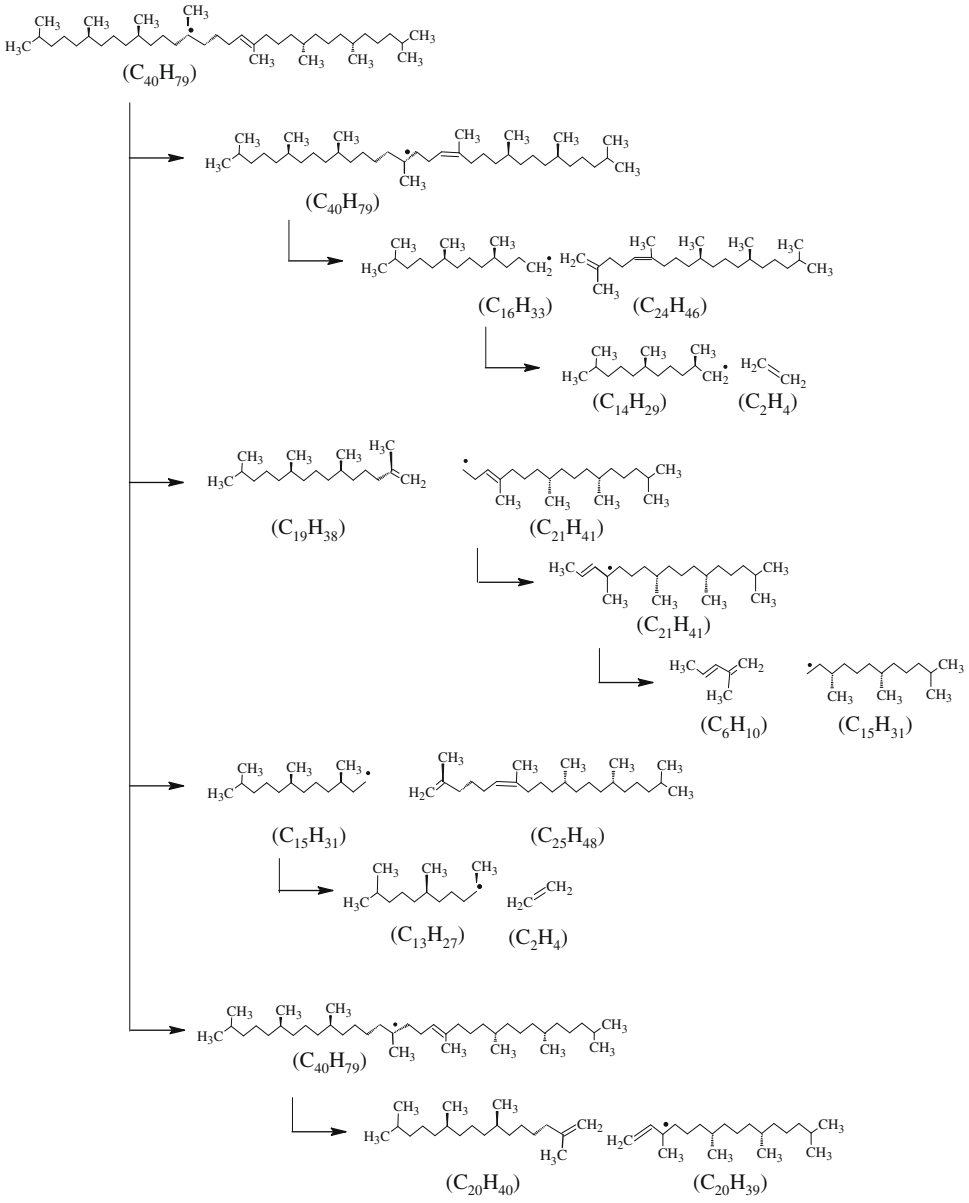

Fig. 10. β-Scission reactions of the isoprenoid side chain ($C_{40}H_{79}$) as observed in the constant temperature simulations of the algaenan macro-model.

Table 4
Chemical composition observed after 37 ps of NVT-MD simulation at T = 1500, 1600, 1700, 1800, 1900, and 2000 K of the algaenan macro-models.

Algaenan macromodel $C_{1037}H_{1900}O_{29}$						
	1500 K/37 ps	1600 K/37 ps	1700 K/37 ps	1800 K/37 ps	1900 K/37 ps	2000 K/37 ps
C_{40+}compounds	1 $C_{526}H_{933}O_{19}$	1 $C_{487}H_{845}O_{21}$	1 $C_{488}H_{845}O_4$	1 $C_{160}H_{282}O_4$	1 $C_{169}H_{296}O_6$	1 $C_{132}H_{229}O_4$
	1 $C_{189}H_{335}O_6$	1 $C_{186}H_{335}O_6$	1 $C_{159}H_{335}O_6$	1 $C_{125}H_{216}O_6$	1 $C_{155}H_{274}O_4$	1 $C_{90}H_{157}O_2$
				1 $C_{96}H_{168}O_3$	1 $C_{107}H_{191}O_4$	1 $C_{64}H_{112}O_2$
				1 $C_{82}H_{145}O_3$	2 $C_{63}H_{110}O_2$	1 $C_{59}H_{102}O_2$
				1 $C_{55}H_{98}$		1 $C_{58}H_{107}O_2$
						1 $C_{57}H_{102}O$
				1 $C_{42}H_{75}O$		
C_{40-}compounds	8 $C_{40}H_{79}$*	9 $C_{40}H_{79}$*	9 $C_{40}H_{79}$*	8 $C_{40}H_{79}$	4 $C_{40}H_{79}$*	4 $C_{40}H_{79}$*
					1 $C_{33}H_{59}O$	1 $C_{33}H_{59}O$
				1 $C_{31}H_{55}$	1 $C_{31}H_{55}$	
				1 $C_{28}H_{53}$	1 $C_{29}H_{51}$	1 $C_{28}H_{53}$
				1 $C_{27}H_{47}$		1 $C_{27}H_{47}$
					3 $C_{25}H_{48}$*	3 $C_{25}H_{48}$*
					1 $C_{24}H_{46}$*	1 $C_{24}H_{46}$*
				1 $C_{20}H_{40}$*	1 $C_{20}H_{40}$*	1 $C_{22}H_{40}$*
				1 $C_{20}H_{39}$*	1 $C_{20}H_{39}$*	1 $C_{20}H_{39}$*
				1 $C_{19}H_{38}$*	1 $C_{18}H_{35}$*	1 $C_{19}H_{38}$*
					1 $C_{16}H_{33}$*	1 $C_{18}H_{32}$*
					1 $C_{13}H_{27}$	1 $C_{15}H_{31}$*
C_6–C_{14}compounds						1 $C_{14}H_{29}$*
						1 $C_{13}H_{21}$
					2 $C_{13}H_{27}$*	3 $C_{13}H_{27}$*
						1 C_9H_{15}
C_6-compounds						1 C_6H_{10}*
						1 C_5H_6O
						1 C_4H_6
						1 C_3H_6
				3 C_2H_4	4 C_2H_4	18 C_2H_4
	2 CO_2	1 CO_2		6 CO_2	5 CO_2	7 CO_2

* Denoted isoprenoid structures.

Table 5
Time and temperature conditions for the formations of the main products originated from the decomposition of algaenan race L as obtained from the simulations and from experiment.

Chemical compounds	Numerical observations		Experimental observations	
	T (K)	t (ps)	T (K)	t (h)
$C_{40}H_{79}$	>1400	17	<473	9
CO_2	>1950	27	<473	9
C_2H_4	>2340	32	>573	9
CH_4	–	–	>523	9

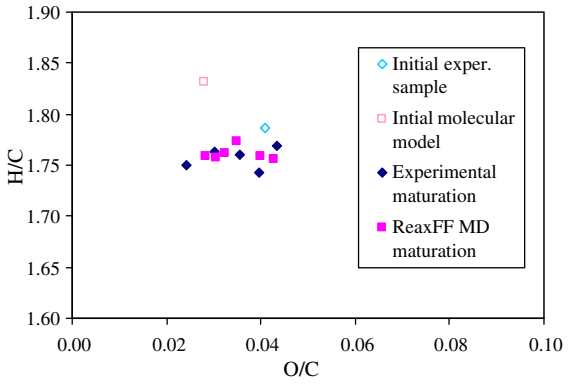

Fig. 11. Influence of thermal stress on the atomic composition as observed in experimental pyrolysis residue and in the C_{40+} hydrocarbons fraction during the NVT-MD simulations.

Acknowledgements

The computational facilities used for this research were provided by grants from DARPA-ONR and DARPA-ARO. Other support was provided by ONR (N00014-05-1-0778) and by GeoForschungs-Zentrum Potsdam (GPM 200700350). We also thank Jim Kubicki and Thomss Sewell for their constructive review of this manuscript.

Associate Editor—**Clifford Walters**

References

Behar, F., Derenne, S., Largeau, C., 1995. Closed pyrolyses of the isoprenoid algaenan of *Botryococcus braunii*, L race: Geochemical implications for derived kerogens. Geochimica et Cosmochimica Acta 59, 2983–2997.

Berendsen, H.J.C., Postma, W.F., van Gunsteren, A., Dinola, A., Haak, J.R., 1984. Molecular dynamics with coupling to an external bath. The Journal of Chemical Physics 81, 3684–3690.

Berthéas, O., Metzger, P., Largeau, C., 1999. A high molecular weight complex lipid, aliphatic polyaldehyde tetraterpenediol polyacetal from *Botryococcus braunii* (L race). Phytochemistry 50, 85–96.

Brenner, D.W., 1990. Empirical potential for hydrocarbons for use in simulating the chemical vapour deposition of diamond films. Physical Review B 42, 9458–9471.

Buehler, M.J., van Duin, A.C.T., Goddard III, W.A., 2006. Multiparadigm modeling of dynamical crack propagation in silicon using a reactive force field. Physical Revue Letters 96, 095505.

Chen, N., Lusk, M.T., van Duin, A.C.T., Goddard III, W.A., 2005. Mechanical properties of connected carbon nanorings via molecular dynamics simulation. Physical Revue B 72, 085416.

Chenoweth, K., Cheung, S., van Duin, A.C.T., Goddard III, W.A., Kober, E.M., 2005. Simulations on the thermal decomposition of a poly(dimethylsiloxane) polymer using the ReaxFF Reactive Force Field. Journal of American Chemical Society 127, 7192–7202.

Chenoweth, K., van Duin, A.C.T., Goddard III, W.A., 2008. ReaxFF reactive force field for molecular dynamics simulations on hydrocarbon combustion. Journal of Physical Chemistry A 112, 1040–1053.

Chopra, M., Malshe, R., Reddy, A.S., de Pablo, J.J., 2008. Improved transition path sampling methods for simulation of rare events. Journal of Chemical Physics 128 (14), 144104.

Freund, H., Walters, C.C., Kelemen, S.R., Siskin, M., Gorbaty, M.L., Curry, D.J., Bence, A.E., 2007. Predicting oil an gas compositional yields via chemical structure-chemical yield modelling (CS-CYM): part 1 – concepts and implementation. Organic Geochemistry 38, 288–305.

Goddard III, W.A., Merinov, B., van Duin, A.C.T., Jacob, T., Blanco, M., Molinero, V., Jang, S.S., Jang, Y.H., 2006a. Multi-paradigm multi-scale simulations for fuel cell catalysts and membranes. Molecular Simulation 32, 251–268.

Goddard III, W.A., van Duin, A.C.T., Chenoweth, K., Cheng, M.-J., Pudar, S., Oxgaard, J., Merinov, B., Jang, Y.H., Persson, P., 2006b. Development of the ReaxFF reactive force field for mechanistic studies of catalytic selective oxidation processes on BiMoOx. Topics in Catalysis 38, 93–103.

Han, S.S., van Duin, A.C.T., Goddard III, W.A., Lee, H.M., 2005. Optimization and application of lithium parameters for the reactive force field, ReaxFF. Journal of Physical Chemistry A 109, 4575–4582.

Huck, G., Karweil, J., 1955. Physikalische Probleme der Inkohlung. Brennstoff-Chemie 36, 1–11.

Karweil, J., 1955. Die Metamorphose der Kohlen vom Standpunkt der physicalischen Chemie Zeitschrift der Deutschen Geologischen Gesellschaft 107, 132–139.

Kelemen, S.R., Freund, H., Siskin, M., Carry, D.J., Xiao, Y., Olmstead, W.N., Gorbaty, M.L., Bence, A.E., 2004. Chemical structural and composition yields model for predicting hydrocarbon thermolysis products. US Patent Publication No. 2004/0019437 ExxonMobil Upstraem Research Co., Houston, TX (assignee), 21 claims, 10 pp.

Leininger, J.-P., 2007. Stabilité thermique de composés hydroaromatiques et aromatiques des fluides pétroliers : Etude experimentale, modélisation théorique et cinétique. Thèse de doctorat de l'Université Pierre et Marie Curie, 253.

Leininger, J.-P., Minot, C., Lorant, F., 2008. Two theoretical simulations of hydrocarbons thermal cracking: Reactive force field and density functional calculations. Journal of Molecular Structure: THEOCHEM 852, 62–70.

Lopatin, N.V., 1971. Temperature and geological time as factors of carbonification. Akademiya Nauk SSSR Izvestiya, Seriya Geologicheskaya 3, 95–106.

Ludwig, J., Vlachos, D.G., van Duin, A.C.T., Goddard III, W.A., 2006. Dynamics of the dissociation of hydrogen on stepped platinum surfaces using the ReaxFF Reactive Force Field. Journal of Physical Chemistry B 110, 4274–4282.

Mortier, W.J., Ghosh, S.K., Shankar, S.J., 1986. Electronegativity-equalization method for the calculation of atomic charges in molecules. Journal of American Chemical Society 108, 4315.

Payne, D.F., Ortoleva, P.J., 2002a. A model for lignin alteration—part I: a kinetic reaction-network model. Organic Geochemistry 32 (9), 1073–1085.

Root, D.M., Landis, C.R., Cleveland, T., 1993. Valence bond concepts applied to the molecular mechanics description of molecular shapes. 1. Application to nonhypervalent molecules of the p-block. Journal of American Chemical Society 115, 4201–4209.

Root, M.D., 1997. Valence bond principles applied to the molecular mechanics description of molecular shapes. PhD Thesis. The University of Wisconsin – Madison, Source DAI-B 57/12, p. 7525, June 1997, 178 pp.

Rappé, A.K., Casewit, C.J., Colwell, K.S., Goddard III, W.A., Skid, W.M., 1992. UFF, a full periodic table force field for molecular mechanics and molecular dynamics simulations. Journal of American Chemical Society 114, 10024–10039.

Rappé, A.K., Goddard III, W.A., 1991. Charge equilibration for molecular-dynamics simulations. Journal of Physical Chemistry 95, 3358–3363.

Salmon, E., Behar, F., Lorant, F., Hatcher, P.G., Metzger, P., Marquaire, P.-M., 2009. Thermal decomposition process in algaenan of *Botryococcus braunii* race L. Part 1: experimental data and structural evolution. Organic Geochemistry 40, 400–415.

Savage, P.E., Klein, M.T., 1989. Asphaltene reaction pathways – V. Chemical and mathematical modeling. Chemical Engineering Science 44, 393–404.

Solomon, P.R., Hamblen, D.G., Carangelo, R.M., Serio, M.A., Deshpande, G.V., 1988. General model of coal devolatilization. Energy & Fuels 2, 405–422.

Strachan, A., van Duin, A.C.T., Chakraborty, D., Dasgupta, S., Goddard III, W.A., 2003. Shock waves in high-energy materials: the initial chemical events in nitramine RDX. Physical Revue Letters 91, 098301.

Tersoff, J., 1988. New empirical approach for the structure and energy of covalent systems. Journal of Physical Revue B 37, 6991.

Tissot, B., 1969. Premières données sur les mécanismes et la cinétique de la formation du pétrole dans les bassins sédimentaires. Simulation d'un schéma réactionnel sur ordinateur. Oil & Gas Science and Technology 24, 470–501.

Tissot, B., 1973. Vers l'évaluation quantitative du pétrole formé dans les bassins sédimentaires. Revue Association Français Technologie Pétrole 222, 27–31.

Van Duin, A.C.T., Dasgupta, S., Lorant, F., Goddard III, W.A., 2001. ReaxFF: a reactive force field for hydrocarbons. Journal of Physical Chemistry A 105, 9396–9409.

Van Duin, A.C.T., Sinninghe Damsté, J.S., 2003. Computational chemical investigation into isorenieratene cyclisation. Organic Geochemistry 34, 515–526.

Van Duin, A.C.T., Zeiri, Y., Dubnikova, F., Kosloff, R., Goddard III, W.A., 2005. Atomistic-scale simulations of the initial chemical events in the thermal initiation of triacetonetriperoxide. Journal of American Chemical Society 127, 11053–11062.

Vassoevich, N.B., Korchagina, Yu, I., Lopatin, N.V., Chernyshev, V.V., 1969. Principal phase of oil formation. Moskow Univ. Vestnik 6, 3-6 (in Russian), English Translation. International Geology Review 12, 1276–1296.

Waples, D.W., 1980. Time and temperature in petroleum formation/application of Lopatin's method to petroleum exploration. American Association of Petroleum Geologists Bulletin 64, 916–926.